Photoselective Ultrafast Investigation of Xanthorhodopsin and Its Carotenoid Antenna Salinixanthin

Jingyi Zhu,[†] Itay Gdor,[†] Elena Smolensky,[‡] Noga Friedman,[‡] Mordechai Sheves,[‡] and Sanford Ruhman*[,†]

Institute of Chemistry and the Farkas Center for Light Induced Processes, The Hebrew University, Jerusalem 91904, Israel, and Department of Organic Chemistry, Weizmann Institute of Science, Rehovot 76100, Israel

Received: November 14, 2009; Revised Manuscript Received: January 19, 2010

Excited-state dynamics of xanthorhodopsin (XR) and of salinixanthin (SX) in ethanol were investigated by ultrafast pump−hyperspectral probe spectroscopy. Following excitation to the strongly allowed S_2 state of the SX chromophore, transient spectra were recorded photoselectively in the range 430−850 nm. Global kinetic analysis of these data shows the following. (1) Efficient energy transfer from S_2 of the SX in XR to its retinal moiety is verified here. The lifetime of S_2 in SX is, however, determined to be ∼20 fs, much shorter than previously reported. (2) Branching ratios of excitation transfer from S_2 to S_1, to S*, and to retinal in XR are measured leading to species associated difference spectra (SADS) for all the states involved. Strong protein effects are detected on these branching probabilities. (3) S_1 and S* absorption bands in both systems exhibit anisotropy well below the expected $r = 0.4$, indicating an angle of ∼25° between the $S_0 \rightarrow S_2$ and $S_1 \rightarrow S_n$/S* → S_n transition dipoles. The latter allows confident assignment of the debated S* absorption band to an excited state of SX, and not to "hot" S_0. In light of the extremely fast IC from S_2 to lower excited singlets, possible involvement of ballistic IC in SX, and of coherent energy transfer in XR, are discussed.

Introduction

Xanthorhodopsin (XR) is a light-driven proton pump isolated from the extremely halophilic eubacterium Salinibacter rubber which grows in brine pools and salt lakes.[1,2] It contains two strongly interacting chromophores, an all-*trans*-retinal, and a C40 carotenoid (CAR) salinixanthin (SX) which, aside from stabilizing the protein structure, acts as a light-harvesting antenna.[3,4] Binding the retinal chromophore to the protein pocket nearly doubles the proteins visible absorption cross section,[5] enabling the bacterium to utilize the green and blue parts of the solar spectrum for biological activity as well. Light absorbed by SX is transferred to the retinal chromophore which uses it for transmembrane proton transport, making XR the simplest photosynthetic protein complex featuring a separate light-harvesting function.

Structural and dynamical information concerning the sensitized photocycle of XR has been obtained from steady-state spectroscopy.[6–9] Circular dichroism (CD) measurements and comparison of steady-state spectra of XR before and after lysing of the embedded retinal show that strong cooperative binding effects exists between both chromophores.[10,11] The lysing of the retinal moiety not only eliminates its typical midvisible absorption band but also simultaneously reduces the CAR's absorption cross section, and washes out its sharp vibronic structure. Polarized fluorescence measurements demonstrate that the CAR transition dipole moment is oriented at about 56° relative to that of the retinal,[8] in near agreement with the value of 46° angle between the molecular axes later obtained by X-ray crystallography.[9] The latter also reveals a center to center distance between both chromophores of ∼11 Å. This close approach and favorable alignment are presumably responsible for the high energy transfer (ET) efficiency in XR, which was measured to be between 30% and 50%.[3,4,8] Energetics of both chromophores, along with quantum yields of emission in XR and SR in solution, suggest the ET route to be from the CAR S_2 state to the reactive retinal S_1. This assignment requires the process of ET to be extremely fast, as internal conversion of the bright S_2 state in CARs of this size is already subpicosecond even without competing relaxation channels.[12,13]

In order to directly follow the process of ET and retinal isomerization in this protein complex, a comparative spectroscopic study of the native XR and of its isolated light-harvesting CAR in solution was initiated in our lab. For this purpose, state of the art ultrafast spectroscopic methods, including a sub-10 fs laser source, were utilized, allowing the resolution of even the fastest inter- and intramolecular relaxation processes. In view of the important part polarization methods played in the CW studies, all experiments were upgraded to allow selection of relative pump and probe polarization orientations.

During the course of this study, an ultrafast spectroscopy study of XR and SX with similar objectives was published by Polivka et al.[14] Their experiments demonstrated the ultrafast and efficient nature of CAR to retinal ET, justifying the assignment of S_2 as the donor state. The time scale for isomerization of the retinal following sensitization was also determined and shown to be somewhat slower than the equivalent process in bacteriorhodopsin. Based upon the comparison of magic-angle pump−probe results in native XR with those obtained from a protein suspension where the retinal is reduced and spectrally shifted, an energy relaxation and transfer mechanism was suggested for XR, with an ET rate of $K_{ET} = 6 \times 10^{-3}$ fs^{-1} between the donor and acceptor, an S_2 lifetime of 66 fs for XR, and ∼120 fs for a sample of XR where retinal has been bleached by reduction.

Our results agree in part with those reported by Polivka and co-workers. These include the overall scheme of ET, as well as the relaxation rates associated with the later phases of kinetic

* Corresponding author. E-mail: sandy@fh.huji.ac.il.
[†] The Hebrew University.
[‡] Weizmann Institute of Science.

10.1021/jp910845h
Published on Web 02/10/2010

evolution. Superior time resolution and photoselective probing used here have, however, provided novel insights which relate both to the mechanisms of ET, and the nature of the reactive intermediates. Spectra of all relevant photointermediates in XR and isolated SX, along with their polarization anisotropies, are extracted from the transient absorption experiments using global fitting analysis. The results demonstrate that the CAR donor state is much shorter lived than previously reported, and gives way through internal conversion to two electronically excited intermediates (S_1,S*), both of which exhibit absorption bands polarized at ~25° to that of the ground state. The implications of these results concerning the dynamics of ET to retinal in XR and the identity of the S* state are discussed.

Experimental Methods

Sample Preparation. Growth of *S. ruber* was carried out according to published methods[1,3] with the addition of 0.1% sucrose according to ref 15. XR membranes samples were isolated using previously described procedure.[11] The membranes were washed with 0.01% of dodecylmaltoside (DM) followed by washing three times with DDW. The membranes were resuspended in 0.01% dodecylmaltoside (DM). To reduce the excess of unbound salinixanthin, an aerated membranes suspension was reacted with 20 mM $NaBH_4$ in the dark such that ca. 25% percent of the salinixanthin absorbance was reduced. This treatment bleached mainly the unbound salinixanthin and did not reduce the protonated Schiff base linkage. $NaBH_4$ was removed by a dialysis process.

Extraction of Salinixanthin. Membrane suspension of XR (0.3 OD at 486 nm, 6 mL) was denaturated by vigorously mixing the pigment with EtOH (12 mL) and acetone (25 mL). Salinixanthin was extracted with hexane (140 mL), and the carotenoid was further purified by silica gel chromatography (acetone/hexane, 2:3) according to a published method.[16]

UV−Visible Absorbance Measurements. All the absorbance measurements were carried out using a Agilent 4583 diode-array spectrophotometer (Agilent Technologies, Palo Alto, CA) equipped with an Agilent 89090A thermostated cuvette holder. Absorption spectra were corrected for light scattering.

Pump−Probe Measurements. A room temperature sample was syringe pumped through a 0.4 mm path length flow cell equipped with 0.1 mm glass windows. The concentrations of XR and SX in ethanol produced nominal OD of 0.7 and 0.5 at 480 nm, respectively. The integrity of the sample was determined by measuring its absorption spectrum before and after each run. The laser system and methods of measurement have been described in detail elsewhere.[17] Thirty femtosecond pulses centered at 790 nm and containing 0.5 mJ were derived from a homemade titanium sapphire multipass amplifier. Part of the laser pulse energy was used to generate a multifilament white light continuum probe by focusing the beam in 1.5 mm of sapphire. The continuum pulses were split into probe and reference beams, and the latter collimated and refocused into the sample with reflective optics. The remaining fundamental was used to pump a TOPAS (Light Conversion) and produce 20 fs pump pulses centered at 480 nm by mixing signal with amplifier fundamental. 250 nJ of the resulting pulse was focused in the sample to a spot of ~200 μm in diameter. Kerr scans in water provided the probes λ-dependent group delay and indicated a pump−probe cross correlation of 60−80 fs throughout the probed range.

Parallel and perpendicular pump−probe polarizations were achieved using a calcite Glan laser polarizer on the continuum generating 790 nm probe and an achromatic half-wave plate (special optics) and low-dispersion polarizer (Colorpol) combination in the pump beam. Dispersion was compensated in a slightly misaligned zero-dispersion grating pulse shaper, also employed to cut off the pump pulse spectral wings in order to reduce the impact of pump scatter. Probe and reference pulses were collected by fibers into a double spectrometer setup to generate the time-dependent difference spectra. After the resulting spectra were corrected for group delay dispersion of the probe continuum, they were analyzed using singular value decomposition (SVD) combined with model-based global fitting.[18]

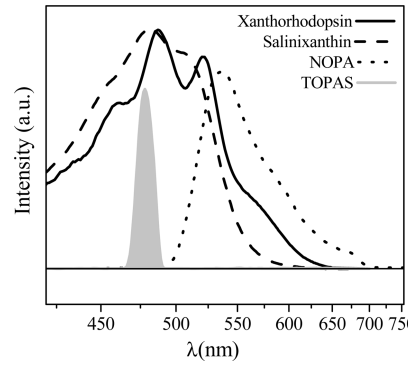

Figure 1. Ground-state absorption spectra of xanthorhodopsin in buffer and salinixanthin in ethanol along with pump intensity spectra of the TOPAS and NOPA

Sub-10 fs time resolution experiments were preformed with an equivalent amplifier, pumping a one-stage noncollinear optical parametric amplifier (NOPA) as described in earlier publications.[19,20] The NOPA output was tuned to the blue in order to maximize the intensity of overlap with the SX absorption spectrum. The resulting output contained 4 μJ of energy per pulse, with a spectrum ranging from 480 to 660 nm corresponding to a 8 fs pulse duration (see Figure 1). The pump beam polarization was adjusted without dispersive elements by a 45° periscope, allowing the transient absorption spectrum to be recorded photoselectively.

Results

The ground-state absorption spectra of XR, and of SX in ethanol, are shown in Figure 1. As reported in previous studies,[4] the absorption spectrum of XR is a combination of its two constituent chromophores. The bound retinal chromophore contributes a broad absorption peaking at ~560 nm due to the excitation from the ground state to the first excited state. This band partially overlaps the strong $S_0 \rightarrow S_2$ CAR spectrum which is much more structured when cobound with the retinal as demonstrated by comparison with the absorption of free SX also depicted in Figure 1. The pump pulses derived from the TOPAS and used to excite both samples are also depicted in gray in the Figure. The central wavelength of 480 nm was chosen for strong resonance with the SX chromophores' absorption, and minimal simultaneous contributions from retinal absorption. Due to spectral overlap, direct absorption of the retinal is unavoidable, and is estimated from the spectrum alone to be responsible for up to 25% of the absorbed photons.

Color-coded three-dimensional maps of transient difference spectra obtained from XR and SX in ethanol are presented in Figure 2. The lower panels show sequences of temporal cuts in the maps above, at delays which are detailed in the legend. Immediately following photoabsorption, increased transmission is observed in both samples, from the blue edge of the probing

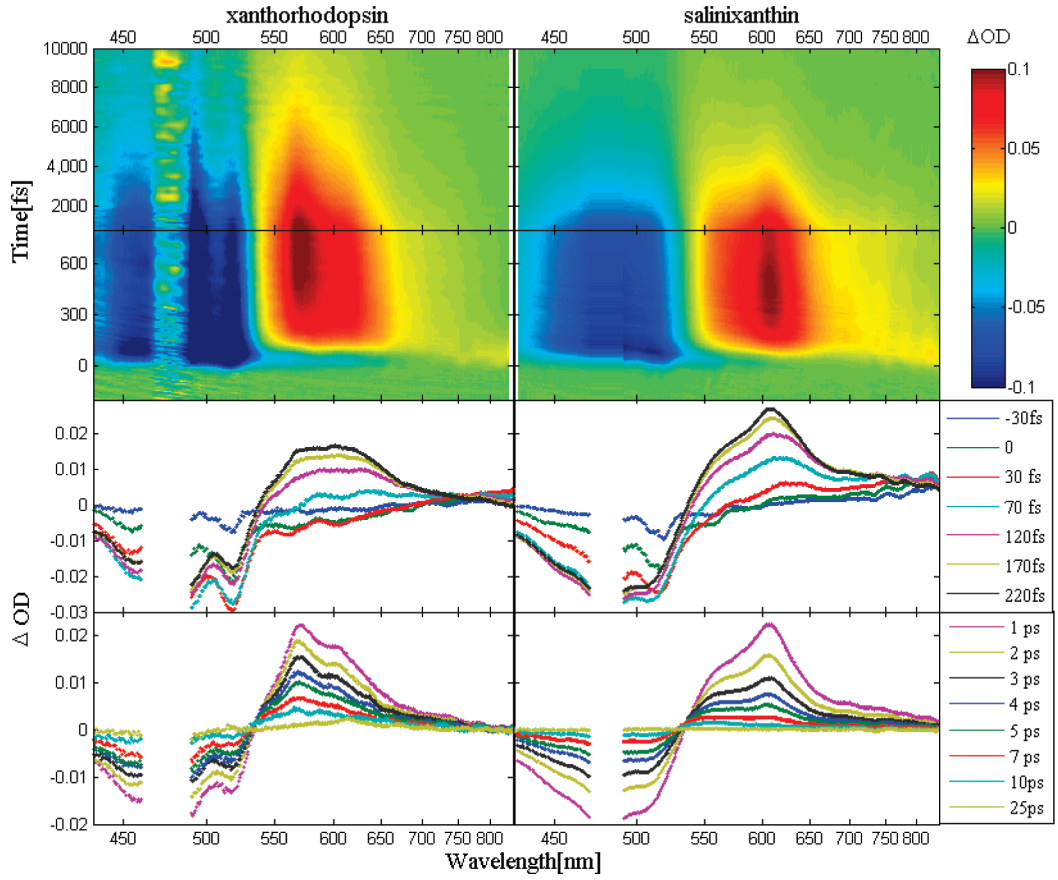

Figure 2. Contour maps of transient difference spectra in xanthorhodopsin and salinixanthin, excited at 480 nm. Below is a sequence of slices in the data taken at the designated pump−probe delays.

range, to ~750 nm. Above this wavelength, an immediate buildup of absorption, extending to the other end of the observation window, is observed. These features decay rapidly, leaving increased transmission in the range where SX absorbs, with a sharp transition to absorption from ~580 nm to the red edge of the probed spectrum. These features evolve spectrally, and decay on picosecond time scales. In the case of SX this decay leads to an effective erasure of the difference spectrum, while in XR a weak residual spectrum is observed. Aside from the long time XR residual, the general appearance of the transient spectra and the time scales of evolution are similar.

In order to investigate the exited-state dynamics, global fitting analysis was performed, including convolution with an experimentally determined Gaussian instrument response function, and four phases of exponential spectral evolution. Both data sets were fit to a sequential kinetic scheme summarized as A → B → C → D → E, A being the initial excited state. The resulting magic angle evolution associated difference spectra (EADS)[18] ($(\Delta OD_{VV} + 2\Delta OD_{VH})/3$) are shown in the two panels of Figure 3 along with the associated rate constants. Similar optimal rate constants are obtained by the fitting procedure for free SX and for XR samples. Note that this model is not suggested as a kinetic mechanism, but rather as a convenient vehicle for representing the separable stages of spectral evolution. In fact, a branched reaction mechanism will be promoted later for explaining the photochemistry of both systems.

The similarity of data from both samples reflects the dominant contribution of the CAR on the transient spectra, a dominance which is clearly observable in the spectra of Figure 1. Previous studies of CAR photophysics allow a loose assignment of the shortest EADS in Figure 3 primarily to internal conversion of

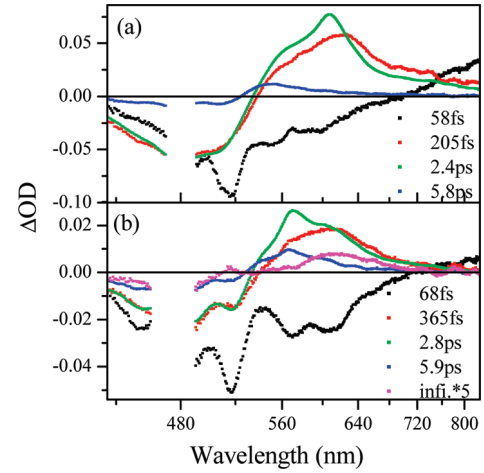

Figure 3. Evolution-associated difference spectra and time constants extracted by global kinetic analysis of the data presented in Figure 2 for SX (a) and XR (b).

the S_2 to lower lying dark excited states. The ~60 fs decay rate which optimally fits data in both samples is very near our limits of resolution in the TOPAS experiments—a point which will be revisited below. The latter stages of evolution can accordingly be ascribed to electronic relaxation of CAR dark excited states back to S_0. The residual long-term photoproduct in the case of XR provides evidence for retinal photocycle sensitization by ET from SX.

In order to extract retinal contributions to the transient difference spectra, data was collected photoselectively with both VV and VH pump−probe polarization alignments. The rationale for this is as follows. Assuming all CAR transitions to be

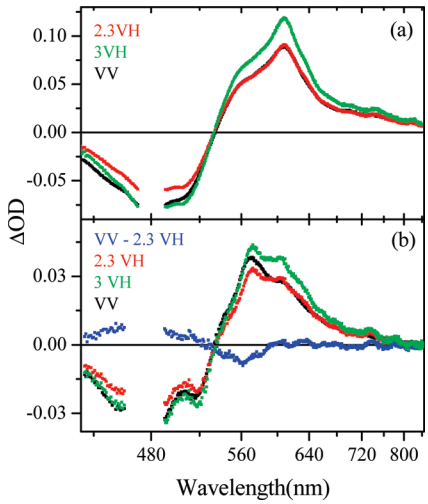

Figure 4. Comparison of VV and VH transient spectra of xanthorhodopsin and salinixanthin obtained at a delay of 1 ps. The VV data is depicted in black, while the VH data is presented after multiplication by two factors, 3 in green, and 2.3 in red. The blue line in (b) is the difference of 2.3 VH−VV assigned to retinal excited by energy transfer from the carotenoid.

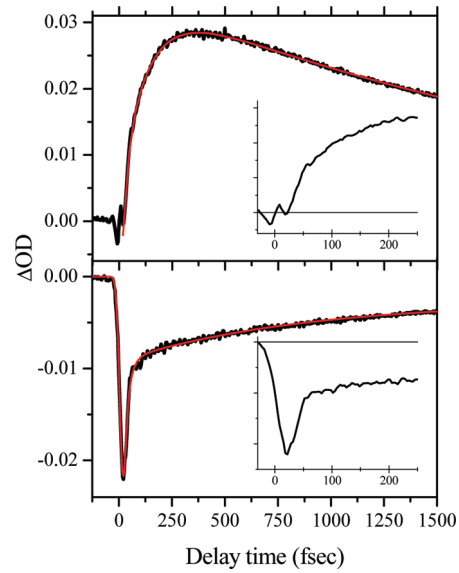

Figure 5. High time resolution NOPA pump, dispersed NOPA probe data at two wavelengths, 600 nm (a), and 520 nm (b). Red lines are biexponential fits including convolution with a 13 fs fwhm Gaussian instrument function. The faster decay constant obtained by fitting is ~20 fs at both wavelengths.

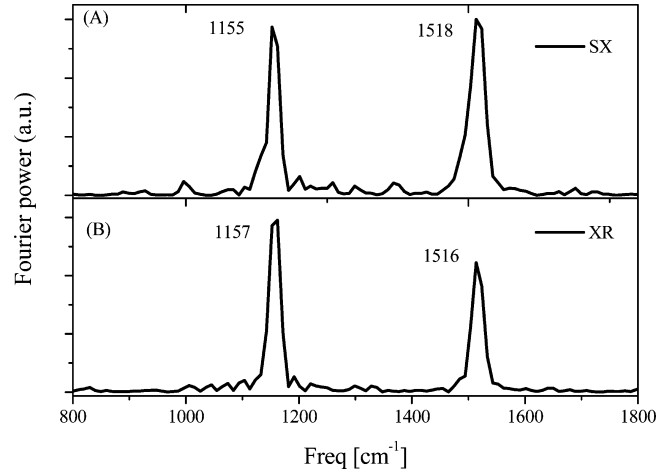

Figure 6. Fourier analysis of spectral modulations extracted from data such as that displayed in Figure 5, by subtraction of the fit from SX data (A) and XR data (B).

polarized along the molecular axis,[21] the SX contributions to VH spectra should be simple replicas of those made to VV, with a constant ratio of 1/3, as expected for conservation of pump and probe dipole moment directions. Retinal transitions are *known* to be polarized along the molecular backbone, but given the nearly "magic" angle between the axes of the two molecules, the sensitized retinal bands should contribute nearly identically to the VV and VH data. Accordingly, a correct subtraction of $3\Delta OD_{VH} - \Delta OD_{VV}$ should allow isolation of the retinal signals. Figure 4 plots ΔOD_{VV} with $3\Delta OD_{VH}$ for the same pump−probe delay of 1 ps. This delay is chosen since ET should already have taken place, but the retinal photocycle has not, and excited-state difference bands should be strong. Strangely, even in the experiments on isolated SX, no single multiplication factor can bring the VV and VH data to coincide across the board. A ratio of 3 works fine for the region of SX ground-state bleach, while a 2.3 ratio fits the strong absorption band tentatively assigned to CAR S_1, as shown in Figure 4, a and b. Using this ratio instead of 3 allows isolation of retinal difference signal, exhibiting a strong bleach maximum at ~560 nm, directly demonstrating the occurrence of ET from the SX to the retinal chromophore. The inability of a single ratio to overlap VV and VH data of SX shows that some of the assumptions above must be incorrect, requiring the more elaborate analysis described in the next section.

In view of the marginal resolution of the initial phase of spectral evolution in the TOPAS data, high time resolution pump−probe experiments with NOPA pulses were conducted. Cuts in the resulting hyperspectral data at $\lambda = 600$ and 520 nm are presented in the upper and lower panels of Figure 5, respectively. The latter follows the rise and decay of the bright S_2 excited state, while the former shows the buildup of the absorptions from the dark excited states. Fitting the SX kinetics at 520 nm to a biexponential decay convoluted with a Gaussian cross correlation of 13 fs gives a much shorter time scale for IC from S_2, no more than 23 ± 5 fs. The same decay constant can be shown to fit the 600 nm data optimally as well. Superimposed on the slower variations in the signals shown in Figure 5, oscillatory fine structure is apparent which after isolation has been Fourier analyzed to produce the power spectra in Figure 6, showing two prominent peaks at 1156 and 1518 cm^{-1} which can be attributed to ground state C−C and C═C stretching, respectively.[22] Peaks at the same two frequencies were uncovered for similar data obtained in a suspension of XR, as shown in the bottom panel of Figure 6.

Target Analysis. A sequential model for XR photochemistry must fail since ET constitutes a mechanistic branching point, and the EADS presented above cannot characterize real species.[18] Even the photochemistry of free CARs has been modeled using branched kinetic schemes.[23,24] In order to make sense out of the unusual polarization results uncovered in data extracted from the TOPAS, modeling must be done in terms of species associated difference spectra (SADS) and time-dependent concentrations. We start with the relatively straightforward analysis of SX spectra. Referring the reader to recent discussions of low-lying dark excited states in large CARs,[25,26] the scheme used to analyze the SX data, and vindicated by the results of this analysis, is summarized in scheme 1of Figure 7. It entails branching through IC of the directly accessed S_2 singlet to two lower lying states coined S_1 and S*. The former is assumed to evolve spectrally in a fraction of a picosecond and convert to

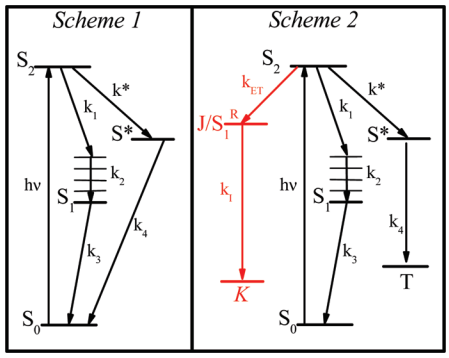

Figure 7. Kinetic schemes used for target analysis of transient spectral data for salinixanthin in ethanol (scheme 1) and for XR (in scheme 2).

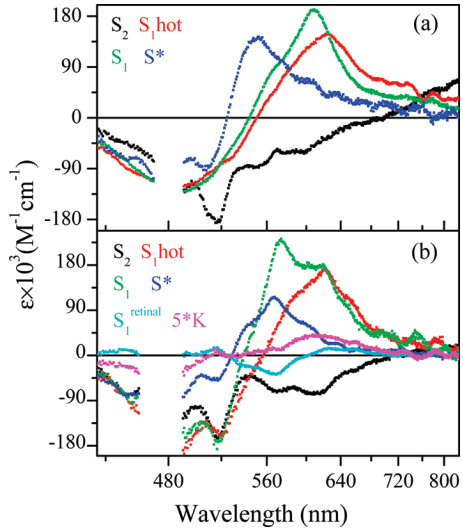

Figure 8. Species associated difference spectra extracted by target analysis using the schemes in Figure 7 for SX (a) and XR (b).

S_0 within a few picoseconds. The latter also repopulates the ground state, albeit more slowly.

In view of the bulkiness of both molecules, and the briefness of the photochemistry, reorientation effects on the polarization measurements can be neglected. One way of obtaining SADS including their λ-dependent polarization ratios is to simultaneously fit VV and VH data sets globally. Here a less rigorous iterative approach is used, starting with target analysis of a synthesized magic angle data set. On the basis of accumulating results on similar CARs, we neglect the absorbance of the S_1 and S* excited states in the range 430−480 nm. Since the SADS of these intermediates include a proportionate S_0 bleach, this assumption amounts to identifying the blue edge of these difference spectra with that bleach exclusively. Assuming that, standard target analysis produced best fitting SADS and associated inverse rate constants which are shown in the top panel of Figure 8 and compiled in Table 1, respectively. According to the stated assumption, the blue edges of the S_1 and S* SADS coincide. This is not true for the S_2-associated spectrum, most likely due to an erroneous determination of the S_2 lifetime. All SADS are determined to within a constant common factor. By scaling these to the extinction values of the ground-state bleach, the real extinction coefficients of each species are obtained in units of $(M \cdot cm)^{-1}$. Aside from the fastest rate constant k_1 which will be discussed explicitly, the resulting rate constants are typical for photoinduced dynamics of CARs containing 13 conjugated double bonds.[12]

TABLE 1: Inverse Rate Constants Extracted from the Global Fitting of SX and XR

	material	
inverse rate constant	SX/ethanol	XR
$1/k_1$	85 ± 12 fs	333 ± 52 fs
$1/k_2$	205 ± 18 fs	256 ± 29 fs
$1/k_3$	2.4 ± 0.1 ps	2.8 ± 0.4 ps
$1/k^*$	221 ± 33 fs	154 ± 24 fs
$1/k_4$	5.8 ± 0.5 ps	5.9 ± 0.7 ps
$1/k_{ET}$		192 ± 30 fs
$1/k_I$		1.2 ps

Having completed the magic angle target analysis, λ-dependent polarization ratios for all the excited states in scheme 1 were derived from the VV and VH polarization experiments. The parallel polarized data set was fit using scheme 1, confined to the reaction rates and branching ratios obtained in fitting the magic angle data. The VH SADS were then derived from the previous two. To eliminate effects of residual noise, particularly in the lower S/N level VH SADS, a smoothing procedure was conducted by least-squares fitting according to the following equation: $SADS_{VH} = SADS_{VV} \times poly^n(\lambda)$. This amounts to fitting the VH SADS to a variably weighted VV SADS, where the weighting factor is a smooth polynomial function of λ. The order of the polynomial n was increased until a satisfactory fit was achieved.

The resulting polynomial is then a best fitting estimate of $1/P(\lambda)$, where $P(\lambda) = (\Delta OD_{VV})/(\Delta OD_{VH})$ is the polarization ratio shown in the panels of Figure 9, along with the matching ratio derived directly from the individual SADS. The λ dependence of the anisotropy can now be credited to specific intermediates. While marginal time resolution with respect to the S_2 lifetime thwarts reliable determination of $P^{S_2}(\lambda)$, only curves showing this measure for nascent and relaxed S_1 and for S* are depicted in Figure 9. Throughout the strong visible absorption bands of all three, a polarization ratio of ~2.3 and not the expected 3 is observed. Such a reduced value of P indicates the existence of an angle between the transition dipoles involved in the pump and probe interactions. In both S_1 SADS, a rise of P toward 3 near the blue S_0 absorption band is observed, but not in S*.

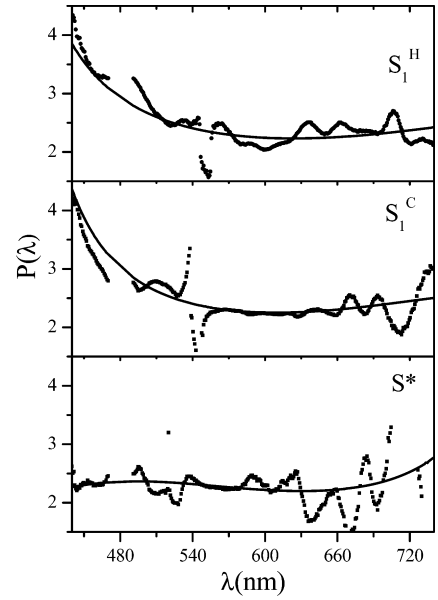

Figure 9. Polarization ratios of the salinixanthine species associated spectra from Figure 8, along with polynomial fits to the data.

Target analysis of the XR results is complicated by ET branching according to scheme 2 in Figure 7 (see previous analysis by Polivka et al.[14]). Use of this scheme requires further assumptions concerning the spectra associated with the additional intermediates. Aside from the previous assumption of identical S_0 bleaching signals dominating S_1 and S* SADS on the blue end, the S_1^R SADS is assumed to have a peak extinction coefficient at 570 nm equal to 1/3 that of the CAR ground-state peak absorption, in accordance with spectra in Figure 1. In separate experiments, the retinal moiety was exclusively excited and the course of IC followed by hyperspectral probing. As shown in the Supporting Information, IC kinetics is approximately monoexponential with $\tau \sim 1.2$ ps. The decay of S_1^R was fixed at this value for XR target analysis. Also employing the estimated 20% direct excitation in the retinal band, XR SADS associated with inverse rate constants in Table 1 were derived and are shown in the bottom panel of Figure 8. The enhanced structure observed in XR SADS relative to equivalent SX spectra is in accord with the differences of CAR bands in the two reactants, shown in Figure 1. Since SX overshadows the retinal at early stages of spectral evolution, a mixture of retinal "I/J" intermediate is reliably extracted for this chromophore. Still, the restricted position and amplitude of the ground-state bleach affords reasonable SADS of SX excited states.

The extensive branching in XR, as well as the spectral overlapping of coexisting transient species, precludes determination of species associated spectral polarization ratios as in the case of SX. Nonetheless, for specific delays, new information can be gleaned from the separate experiments. The dominant extinction coefficients of carotenoid bands, along with the weakness of retinal photoproduct difference absorption spectra[27,28] allow an assignment of a combined $S_1 + S^*$ polarization ratio for $t > 2$ ps. As before, the absorption bands of the CAR excited states again exhibit a P value around 2.3. Clearly the mechanism behind this effect is not altered by inclusion of SX in the protein. Assuming this to be the case for both excited states, this anisotropy value can be used to isolate the retinal excited state contributions due to ET by subtracting 2.3 times the VH from the VV transient spectra. As shown in the blue line of Figure 4b, the subtraction produces a negative absorption band centered at ~570 nm, as expected for the transient difference spectrum of the retinal protein, validating the analysis and interpretation.

Additional products of the analysis are the relaxation rate constants and probabilities of branching from S_2 in the two samples. Since both experimental setups tell a different story concerning S_2 lifetimes, we comment only about the later stages of relaxation. Table 1 shows that inclusion of SX in the protein not only does not effect the decay rate of its S_1 state absorption. It also has little effect on the "cooling" rate of S_1, or on the IC rate of S*. Strangely, the ratio of branching from S_2 *is* affected by SXs' inclusion in the protein. The ratio of branching to S_1 and S* for SX in ethanol is 70/30, while in the protein, branching to S_1, S*, and retinal, are 20/45/35, respectively. Thus inclusion in the protein enhances the relative population of the S* considerably.

The temporal and spectral coverage of the NOPA experiments is insufficient to warrant similar target analysis. It is, however, important to establish the relevance of those experiments to the TOPAS based data collected with lesser time resolution. To demonstrate this, two NOPA/TOPAS data comparisons are provided in Figure 10. Panel (a) presents scaled 520 nm cuts in both data sets, along with a convolution of the NOPA curve with an 80 fs fwhm Gaussian function. In this panel scaling is

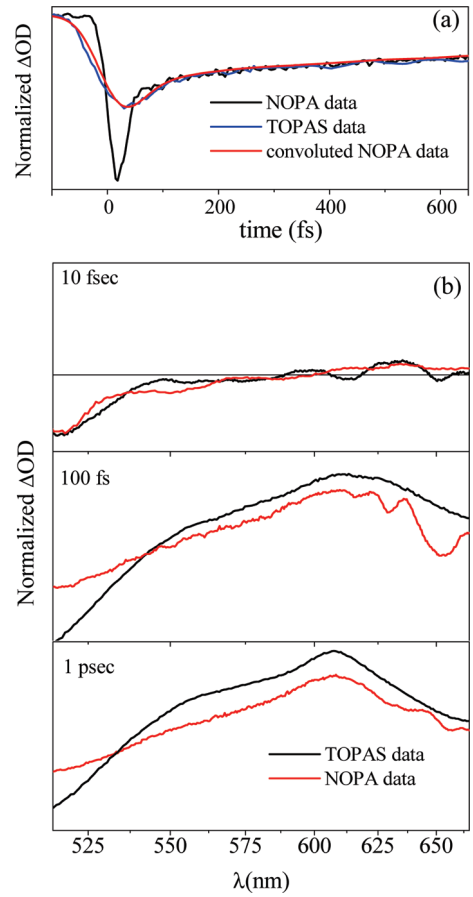

Figure 10. Comparison of NOPA and TOPAS transient spectral data. (a) Kinetics at 520 nm observed with TOPAS (blue), NOPA (black), and after convoluting the latter with a 70 fs fwhm Gaussian function (red). The curves are normalized to coincide at long delays. (b) Transient ΔOD spectra obtained at three different delays using the TOPAS setup (black) and the NOPA (red line).

made to provide overlap of the curves at longer delays. Convolution brings both curves into perfect overlap at all delays, suggesting that differences between the TOPAS and NOPA measurements are due to differences in time resolution afforded by both. The lower three panels compare transient spectra obtained at three different delays on the NOPA system, with equivalent spectra obtained with the TOPAS scaled by a constant factor which brings the 10 fs data into maximal overlap. The results show good agreement between the spectra at all three delays. The resemblance obtained in these comparisons demonstrates that the generated excited states, as well as their subsequent photochemistry, are essentially the same regardless of the different excitation sources. In particular, it shows that despite the discrepancy in assigned lifetimes, the initial change is consistent with an S_2 to S_1 IC.

Discussion

Our results demonstrate that, as stated in earlier studies, SX acts as a light-harvesting antenna in the XR complex. They also uphold the assignment of the transfer route as stemming from the directly excited S_2 state of the carotenoid. While the VV and VH spectra depicted in Figure 4 indicate sensitized formation of excited retinal, polarized measurements afford additional quantitative efficiency measures for this process. Two channels can contribute to the retinal isomerized photoproducts after XR irradiation. The first is direct retinal photoexcitation, and the other is light harvesting and ET. The value of P at the

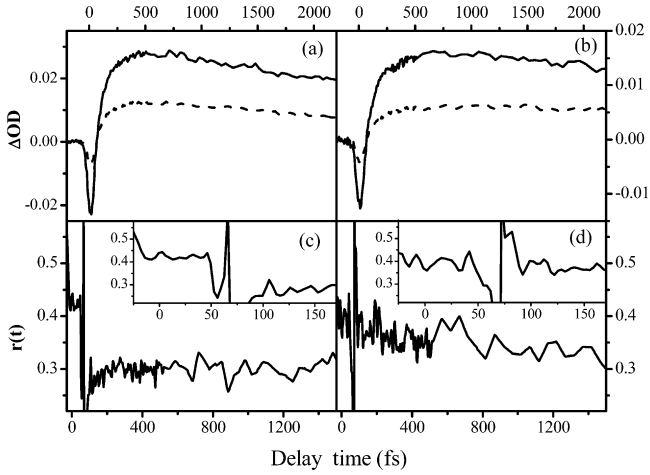

Figure 11. The 550 nm ΔOD kinetics following 480 nm irradiation with parallel (solid) and perpendicular (dashed) pump−probe polarizations in salinixanthine (a) and XR (b). Anisotropies calculated from curves in (a) and (b) are depicted in panels c and d, respectively.

peak of the resulting "K" state absorption is measured to be 1.7, producing an anisotropy value of $r = 0.2$ (Figure S2). While the direct excitation fraction contribution to retinal absorption anisotropy is 0.4, that of ET depends on the angle between the two chromophores, and contributes an average anisotropy value of 0.04. Since they contribute according to the yields of the two channels, the "K" band anisotropy can be calculated as follows:

$$r = \frac{A_{car}\phi}{A_{ret} + A_{car}\phi} \times 0.04 + \frac{A_{ret}}{A_{ret} + A_{car}\phi} \times 0.4 = 0.2$$

where A_{car} and A_{ret} are the directly excited populations of SX and retinal and ϕ is the ET efficiency. Substituting $0.25A_{car} = A_{ret}$ as estimated from the absorption spectra, ϕ is calculated to be 0.32. This value agrees well with the quantum efficiency of 0.35 obtained from target analysis. Since none of the assumptions used in that analysis have been employed, this result provides an independent determination of the probability of energy transfer in this protein.

However, polarization-selective target analysis provides insights extending beyond the validation of earlier models. Starting with SX in solution, the two SADS assigned for nascent and relaxed S_1 preserve an overall band integral as expected, but also exhibit the unusual polarization anisotropy of 0.3. The same is observed for the longer lived S* state. Such a mismatch of pump and probe transition dipole directions has been observed in other CARs,[29−31] but no mechanism for this phenomenon has been identified. Either the S*/S_1 excited states are *formed* with this shifted absorption direction, or it is the result of rapid excited-state dynamics. To resolve this question, the ΔOD anisotropy at 550 nm, the peak of the S*/S_1 absorption, is plotted as a function of delay in Figure 11. Starting at 0.4, a sudden change to 0.3 which takes place on a sub-100 fs time scale, the dynamics of which are obscured by the unstable transition of the signal through zero. Nonetheless, the suddenness of this change excludes the involvement of significant structural alterations such as photoisomerization. In the case of XR, while the limiting anisotropy values are similar, the transition observed is gradual, probably due to the influence of overlapping retinal absorption bands.

Understanding why these transitions are oriented at an angle, and why this angle is preserved in the protein as well, requires further study. But even before these are answered, these findings teach new things about the reactive intermediates. First is identification of S* as an excited, and not a hot, ground state. While this has been suggested before, the reduced r value clearly proves this. The similar value of anisotropy for absorption bands of S*, S_1^H, and S_1^C suggests they are variants of the same electronic state. As observed in other CARs, the S_0 bleach portion of S* SADS is highly structured, much more so than those of hot and relaxed S_1.[32] The similar anisotropy of their difference spectra lends credence to the suggestion that the S* is an S_1 equivalent in a particular conformer of the CAR.[33] Interestingly, no such enhancement in structure is obvious for the S* state within the XR complex. We note that species resolved analysis indicates that the relative yield of S* is higher once SX is attached to the protein. Similar behavior has been reported for other photosynthetic complexes as well.[34] Absorption anisotropy is not the only characteristic of low-lying SX excited states which is curiously unaltered by protein binding. A glance at Table 1 proves that IC rates of both S_1 bands and S* are essentially the same for the free CAR and its bound counterpart. This is in contrast to other examples of protein bound CARs where inclusion in protein complexes drastically changes excited-state lifetimes, particularly for carbonyl-conjugated CAR molecules.[35]

Perhaps the most intriguing finding involves IC of S_2, the excited state most relevant to XR function. Contrary to previous studies, analysis of the TOPAS data assigns identical S_2 lifetimes for SX in the protein and in solution, despite the competing process of energy transfer in the former. While this might be ascribed to medium-specific effects on the rates of IC,[36] the possibility that it is due to insufficient time resolution of the experiments is in fact upheld by the pump−probe experiments conducted on the NOPA system. Comparison of data presented in Figure 10 clarifies this point and suggests that the longer lifetimes previously determined may have suffered from similar limitations. But can this extremely short lifetime be corroborated from other existing measurements? Aside from the recent ultrafast spectroscopic study, the estimates of S_2 lifetimes in SX or XR rely on fluorescence quantum efficiencies. Due to the meager fluorescence quantum yields, the error associated with the ∼70 fs S_2 lifetime in XR was quite large, but not enough to allow for a correct value near 20 fs.

This lifetime for the directly excited state in SX is shorter than any previously reported, even for carbonyl conjugated CARs,[37] and if correct may not reflect the coupling strengths to the lower singlet states. More likely, it reflects steric and inertial barriers to attaining geometry of energetic degeneracy with a lower potential surface. Very brief features have been reported in β-carotene,[38] but their origin is still uncertain.[39] In addition, the spectrum associated with that ∼15 fs feature does not match any of the intermediate states recorded with lesser time resolution. In contrast, as shown in Figure 10, the spectra associated with the shortest stage of evolution in both our experiments are similar, as are those which follow, indicating that they monitor the same states. Predicting S_2 IC rates by Strikler−Berg analysis[40] and fluorescence quantum efficiencies is probably risky when electronic relaxation is so fast, for the reasons cited above. At a distance of 12 Å, the strong interaction between transition dipoles can lead to markedly nonexponential dynamics of IC, including long-lived electronic coherences mediating the reaction.[41,42] The extremely short S_2 lifetime recorded here suggests that these more exotic aspects of ET in

light-harvesting complexes may play a part in XR photochemistry and will be investigated in future experiments.

Conclusion

The ultrafast photoinduced dynamics of native XR, and of its associated carotenoid SX in ethanol, were studied by polarized femtosecond pump−hyperspectral probe spectroscopy with high time resolution. Global fitting and target analyses verify that SX acts as a light-harvesting antenna, transferring energy from the S_2 excited state to retinal with an efficiency of ∼1/3. Lifetimes of the "dark" S_1 and S* singlet excited states were extracted along with their transient difference spectra, and were found to be ∼3 and ∼6 psec respectively for both samples. The cooling time of the nascent S_1 state after its generation by internal conversion from S_2, is also similar in both, taking ∼250 fs.

Individual species associated absorption bands of the carotenoids' S* and S_1 states exhibited unexpectedly low polarization anisotropies, reflecting an angle of ∼25° between the $S_0 \rightarrow S_2$ pump and the $S_1 \rightarrow S_n$ probe transition dipoles. The appearance time of the reduced anisotropy excludes excited state isomerization as its cause. The similar S* absorption polarization ratio bolsters its assignment as an excited and not a hot ground state—probably a specific conformer of the S_1 surface. The surprising polarization ratio for S^*/S_1 absorption bands is maintained when SX is attached to the protein as well.

The lifetime of the bright S_2 excited state in salinixanthin, which facilitates its light-harvesting function, was measured with extreme time resolution and determined to be ∼20 fs, much shorter than previously thought. In light of this ultrashort lifetime, it is likely that coherent nuclear and electronic dynamics are involved in the process of light harvesting, an involvement which remains to be investigated.

Acknowledgment. We thank Ms. Meirav Ben Lulu and Mr. Amir Wand for assistance in NOPA operation, and Prof. A. Oren for providing the strain of *S. ruber*. This work was supported by the Israel Science Foundation (ISF) which is administered by the Israel Academy of Sciences and the Humanities, the US-Israeli Binational Science Foundation, and the Kimmelman center for Biomolecular Structure and Assembly (to M.S.). The Farkas Center is supported by the Minerva Gesellschaft, GmbH, Munich, Germany. M.S. holds the Katzir-Makineni chair in chemistry.

Supporting Information Available: Spectra of xanthorhodopsin at 1 ps delay after direct excitation of the retinal moiety at 590 nm, and transient OD at 560 nm. This material is available free of charge via the Internet at http://pubs.acs.org.

References and Notes

(1) Anton, J.; Oren, A.; Benlloch, S.; Rodrguez-Valera, F.; Amann, R.; Rossell -Mora, R. *J. Syst. Evol. Microbiol.* **2002**, *52*, 485.
(2) Bardavid, R. E.; Ionescu, D.; Oren, A; Rainey, F. A.; Hollen, B. J.; Bagaley, D. R.; Small, A. M.; McKay, C. *Hydrobiologia* **2007**, *576*, 3.
(3) Balashov, S. P.; Imasheva, E. S.; Boichenko, V. A. B.; Anton, J.; Wang, J. M.; Lanyi, J. K. *Science* **2005**, *309*, 2061.
(4) Boichenko, V. A.; Wang, J. M.; Anton, J.; Lanyi, J. K.; Balashov, S. P. *Biochim. Biophys. Acta* **2006**, *1757*, 1649.
(5) Balashov, S. P.; Lanyi, J. K. *Cell. Mol. Life Sci.* **2007**, *64*, 2323.
(6) Imasheva, E. S.; Balashov, S. P.; Wang, J. M.; Lanyi, J. K. *Photochem. Photobiol.* **2006**, *82*, 1406.
(7) Lanyi, J. K.; Balashov, S. P. *Biochim. Biophys. Acta* **2008**, *1777*, 684.
(8) Balashov, S. P.; Imasheva, E. S.; Wang, J. M.; Lanyi, J. K. *Biophys. J.* **2008**, *95*, 2402.
(9) Luecke, H.; Schobert, B.; Stagno, J.; Imasheva, E. S.; Wang, J. M.; Balashov, S. P.; Lanyi, J. K. *Proc. Natl. Acad. Sci.* **2008**, *105*, 16561.
(10) Balashov, S. P.; Imasheva, E. S.; Lanyi, J. K. *Biochemistry.* **2006**, *45*, 10998.
(11) Imasheva, E. S.; Balashov, S. P.; Wang, J. M.; Smolensky, E.; Sheves, M.; Lanyi, J. K. *Photochem. Photobiol.* **2008**, *84*, 977.
(12) Polývka, T.; Sundstrom, V. *Chem. Rev.* **2004**, *104*, 2021.
(13) Kosumi, D.; Yanagi, K.; Fujii, R.; Hashimoto, H.; Yoshizawa, M. *Chem. Phys.Lett.* **2006**, *425*, 66.
(14) Polývka, T.; Balashov, S. P.; Chabera, P.; Imasheva, E. S.; Yartsev, A.; Sundstrom, V.; Lanyi, J. K. *Biophys. J.* **2009**, *96*, 2268.
(15) Oren, A.; Mana, L. *Fems Microbiol. Lett.* **2003**, *223*, 83.
(16) Lutnaes, B. F.; Oren, A; Liaaen-Jensen, S. *J. Nat. Prod.* **2002**, *65*, 1340.
(17) Shoshana, O.; Pérez Lustres, J. L.; Ernsting, N. P.; Ruhman, S. *Phys. Chem. Chem. Phys.* **2006**, *8*, 2599.
(18) Van Stokkum, I. H. M.; Larsen, D. S.; Van Grondelle, R. *Biochim. Biophys. Acta—Bioenerg.* **2004**, *1657*, 82.
(19) Kahan, A.; Nahmias, O.; Friedman, N.; Sheves, M.; Ruhman, S. *J. Am. Chem. Soc.* **2007**, *129*, 537.
(20) Shoshanim, O.; Ruhman, S. *J. Chem. Phys.* **2008**, *129*, 044502.
(21) Orlandi, G.; zerbetto, F.; Zgierski, M. Z. *Chem. Rev* **1991**, *91*, 867.
(22) Koyama, Y.; Long, R. A.; Martin, W. G.; Carey, P. R. *Biochim. Biophys. Acta* **1979**, *548*, 153.
(23) Gradinaru, C. C.; Kennis, J. T. M.; Papagiannakis, E.; Van Stokkum, I. H. M.; Cogdell, R. J.; Fleming, G. R.; Niederman, R. A.; Van Grondelle, R. *Proc. Natl. Acad. Sci.* **2001**, *98*, 2364.
(24) Cong, H.; Niedzwiedzki, D. M.; Gibson, G. N.; Frank, H. A. *J. Phys. Chem. B* **2008**, *112*, 3558.
(25) Papagiannakis, E.; van Stokkum, I. H. M.; Vengris, M.; Cogdell, R. J.; van Grondelle, R.; Larsen, D. S. *J. Phys. Chem. B* **2006**, *110*, 5727.
(26) Polývka, T.; Sundstrom, V. *Chem. Phys. Lett.* **2009**, *477*, 1.
(27) Hasson, K. C.; Gai, F; Anfinrud, P. A. *Proc. Natl. Acad. Sci* **1996**, *93*, 15124.
(28) Gai, F; McDonald, J. C.; Anfinrud, P. A. *J. Am. Chem. Soc.* **1997**, *119*, 6201.
(29) Andersson, P. O.; Gillbro, T. *J. Chem. Phys.* **2005**, *103*, 2509.
(30) Andersson, O. P.; Cogdell, R. J.; Gillbro, T. *Chem. Phys.* **1996**, *210*, 195.
(31) Krueger, B. P.; Lampoura, S. S.; van Stokkum, I. H. M.; Papagiannakis, E.; Salverda, J. M.; Gradinaru, C. C.; Rutkauskas, D.; Hiller, R. G.; van Grondelle, R. *Biophys. J.* **2001**, *80*, 2843.
(32) Chabera, P.; Fuciman, M.; Hrýbeak, P.; Polývka, T. *Phys. Chem. Chem. Phys.* **2009**, *11*, 8795.
(33) Dariusz, M.; Niedzwiedzki; Sullivan, J. O.; Polý'vka, T.; Birge, R. R.; Frank, H. A *J. Phys. Chem. B* **2006**, *110*, 22872.
(34) Papagiannakis, E.; Kennis, J. T. M.; van Stokkum, I. H. M.; Cogdell, R. J.; van Grondelle, R. *Proc. Natl. Acad. Sci.* **2002**, *99*, 6017.
(35) Polivka, T.; Kerfeld, C. A.; Pascher, T.; Sundstorm, V. *Biochemistry* **2005**, *44*, 3994.
(36) Ricci, M.; Bradforth, S. E.; Jimenez, R.; Fleming, G. R. *Chem. Phys. Lett.* **1996**, *259*, 381.
(37) Akimoto, S.; Yokono, M.; Higuchi, M.; Tomo, T.; Takaichi, S.; Murakami, A.; Mimuro, M. *Photochem. Photobiol. Sci.* **2008**, *7*, 1206.
(38) Cerullo, G.; Polli, D.; Lanzani, G.; De Silvestri, S.; Hashimoto, H.; Cogdell, R. J. *Science* **2002**, *298*, 2395.
(39) Kosumi, C. D.; Komukai, M.; Hashimoto, H.; Yoshizawa, M. *Phys. Rev. Lett.* **2005**, *95*, 213601.
(40) Strickler, S. J.; Berg, R. A. *J. Chem. Phys.* **1962**, *37*, 814.
(41) Chachisvilis, M.; Ku1hn, O.; Pullerits, T.; Sundstrom, V. *J. Phys. Chem. B* **1997**, *101*, 7275.
(42) Cheng, Y. C.; Fleming, G. R. *Annu. Rev. Phys. Chem.* **2009**, *60*, 241.

JP910845H